processes

MDPI

Article

Adsorption Process and Properties Analyses of a Pure Magadiite and a Modified Magadiite on Rhodamine-B from an Aqueous Solution

Mingliang Ge [1,2,3], Zhuangzhuang Xi [1], Caiping Zhu [1], Guodong Liang [2], Yinye Yang [3], Guoqing Hu [1], Lafifa Jamal [5] and Jahangir Alam S.M. [1,4,5,6,*]

1 Key Laboratory of Polymer Processing Engineering of Ministry of Education, National Engineering Research Center of Novel Equipment for Polymer Processing, School of Mechanical & Automotive Engineering, South China University of Technology, Guangzhou 510640, China
2 Key Laboratory of Polymeric Composite & Functional Materials of Ministry of Education, Sun Yat-Sen University, Guangzhou 510275, China
3 School of Material Science and Engineering, Guizhou Minzu University, Guiyang 550000, China
4 School of Engineering, The University of British Columbia, Kelowna, BC, V1V 1V7, Canada
5 Department of Robotics & Mechatronics Engineering, University of Dhaka, Dhaka 1000, Bangladesh
6 Department of Computer Science & Engineering, Jessore University of Science and Technology, Jessore 7408, Bangladesh
* Correspondence: mejahangir@scut.edu.cn; Tel.: +86-132-502-54060 or +86-135-339-19779

Received: 11 July 2019; Accepted: 21 August 2019; Published: 25 August 2019

Abstract: The result of an adsorption experiment indicated that the pure magadiite (MAG) and the modified MAG via cetyltrimethylammonium-bromide (CTAB-MAG) possessed pronounced affinity to the Rhodamine-B (Rh-B) dye molecules. CTAB-MAG was synthesized with an ion-exchange method between MAG and cetyltrimethylammonium-bromide (CTAB) in an aqueous solution. The adsorption capacities of CTAB-MAG and MAG on Rh-B were 67.19 mg/g and 48.13 mg/g, respectively; while the pH and the time were 7 and 60 min, respectively; however, the initial concentration of Rh-B was 100 mg/L, and adsorbent dosage was 1 g/L. Whereas, the adsorption capacity of CTAB-MAG was increased by 40% over MAG which indicated that CTAB-MAG can be used as an efficient low-cost adsorbent. Adsorption kinetics were consistent with the pseudo-second-order kinetic equation; the adsorption processes were dominated by film diffusion process which belonged to monomolecular layer adsorption.

Keywords: magadiite; CTAB-Magadiite; rhodamine-B; adsorption process

Highlights

1. Intercalated CTAB-MAG was characterized by ion exchange;
2. Adsorption kinetics were well fitted in pseudo second order model and adsorption processes were dominated by film diffusion process which belonged to monomolecular layer adsorption;
3. Adsorption capacity on Rhodamine-B of CTAB-MAG (67.19 mg/g) was increased by 40% over MAG (48.13 mg/g).

1. Introduction

Many dyes are toxic for human health, and many dyes are widely used in numerous industries; however, a synthetic pink dye called Rhodamine-B (Rh-B) has been widely used as a pigment for textiles, food production, and biological staining (in biomedical research laboratories). But it is difficult to degrade because of stable chemical structure, as can be seen from Figure 1. There are many kinds of methods used to treat wastewater containing Rh-B, such as electrochemical oxidation [1], catalytic

degradation [2], photocatalytic degradation [3], photoelectrocatalytic degradation [4], heterogeneous photo-Fenton degradation [5], and the adsorption method [6] which is the most common way because it is simple to operate, with wide range of options.

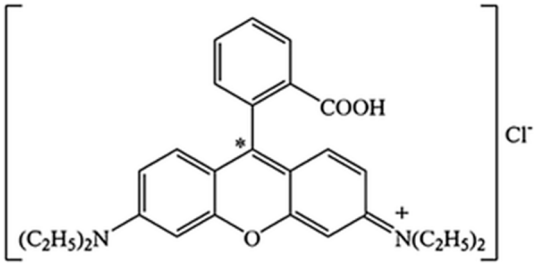

Figure 1. Structure schematic diagram of the Rhodamine-B (Rh-B).

Magadiite (MAG), which was discovered by Eugster in Kenya's saline lake [7], is a natural layered silicate mineral; its plates present a rose petal shape; it presents as a white powder under normal circumstances. There are so many hydrated sodium ions between the plates that the cation-exchange capacity (CEC) is higher than other silicates, such as montmorillonite and can reach up to 2.22 meq/g [8], which was determined from the ideal formulation of MAG ($Na_2Si_{14}O_{29}$). So far, the cation-exchange properties of MAG investigated [9–13], indicate that MAG can be used as an adsorbent, based on cation exchange [14,15]. According to the current study, MAG can be synthesized [16–21]; the laminate of MAG was composed of SiO_4 and has no other impurities. Therefore, the structure of the MAG is very stable and has good chemical stability [22–24]. The Figure 2 shows the lamellar structure of the MAG; the lines of squares, hexagons and octagons, were expressed as Si–O–Si bond [25].

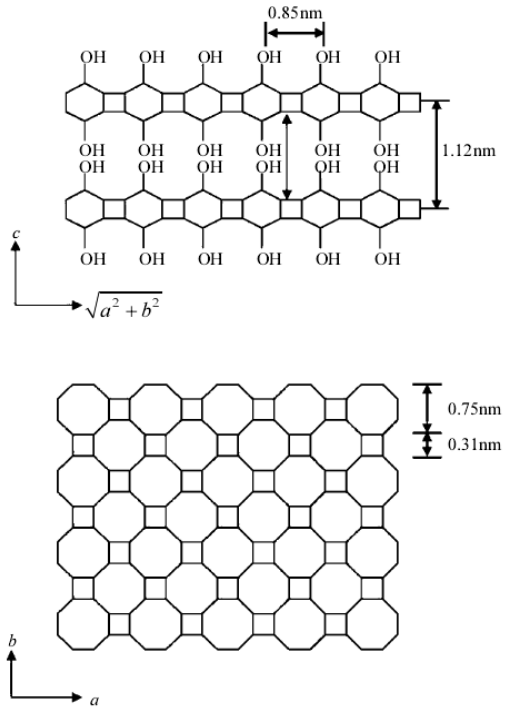

Figure 2. Schematic diagram of the structure of the magadiite (MAG).

So far, there are many ways to modify MAG based on ion exchange. Cetyltrimethylammonium (CTMA) [26,27], heterocyclic ammine [28], and octyl triethoxysilane (OTES) [29] have been used to modify MAG, based on cation exchange, which could effectively expand layer spacing and elevate its adsorption performance. In this experiment, we prepared CTAB-MAG by using

cetyltrimethylammonium-bromide (CTAB) to modify MAG, which can effectively increase the layer spacing of MAG from 1.52 nm to 3.166 nm, thereby enhancing its adsorption capacity, then we used MAG and CTAB-MAG adsorption Rh-B from an aqueous solution to discuss the adsorption mechanism of CTAB-MAG compared with MAG.

2. Experimental

2.1. Experimental Reagents

The Rh-B (chemical pure) and CTAB (chemical pure) were obtained from Tianjin Fuchen Chemical Reagent Factory, (Tianjin, China). Other necessary chemicals (chemical pure) were obtained from Guangzhou Qianhui Company (Guangzhou, China).

2.2. Measuring Instruments

The X-ray diffraction (XRD) analyses were characterized using an AXS D8 ADVANCE X-ray diffractometer (Bruker AXS, Karlsruhe, Germany). Using the range of 500–4000 cm^{-1} at room temperature, the Fourier transform infrared spectroscopy (FTIR) analyses were characterized by a NEXUS 670 type FTIR in a KBr pellet (Nicolet, Waltham, MA, USA). The microscopic surface morphology was observed by SEM analyses by Nova Nano type SEM 430 (Merlin, CA, USA).

2.3. Preparation of Sorbents.

The specific preparation method of MAG was made in our laboratory [21]; the synthesis method of CTAB-MAG was an ion exchange method. The interlayer Na^+ of MAG exchanges with CTA^+ of CTAB to form CTAB-MAG; therefore, the chemical composition of CTAB-MAG was that of the skeleton was MAG, but the interlayer cation was CTA^+. The method of preparation for CTAB-MAG was as follows. First, 5 g MAG was weighed and added to deionized water, 50mL, ultrasonically dispersed for 10 min, and magnetically stirred for 1 h. Then we weighed 2.5 g CTAB and added it to MAG disperse solution. We magnetically stirred the solution with MAG and CTAB at 60 °C for 7 h. We washed the CTAB-MAG solution with deionized water until no foam was visible, and filtered it by suction filtration, then put the CTAB-MAG into a vacuum drying oven and dried at 60 °C for 24 h to obtain CTAB-MAG composite powder.

2.4. Adsorption Performance Experiment

Batch adsorption experimentations were completed to explore the possessions factors of adsorption process in order to investigate the adsorptive performance of MAG and CTAB-MAG on Rh-B, such as initial concentration of Rh-B, contact time, solution pH, and adsorbent dose. After adsorption, the MAG and CTAB-MAG were separated from the Rh-B solution by centrifuge at 6000 rpm/min for 10 min; then the concentration of Rh-B were measured by ultraviolet spectrophotometer [30,31]. The adsorption capacity (q_e) and the removal of Rh-B by the adsorbent is shown in Equations (1) and (2).

$$q_e = (C_0 - C_e) \times V/M \quad (1)$$

$$\text{removal} = (C_0 - C_e)/C_0 \quad (2)$$

where C_0 is the initial concentration of Rh-B (mg/L), C_e is the equilibrium concentration of Rh-B (mg/L), V is adsorption solution volume (mL), and M is adsorbent mass (mg).

2.4.1. Effect of the Initial Concentration of Rh-B

At the normal temperature with the initial concentration of 30, 50, 80, 100, 120, and 150 mg/L, the 40 mL Rh-B solution was added to six beakers; then 40 mg of adsorbent was added for 60 min.

2.4.2. Effect of Adsorption Time

At room temperature, with the initial concentration of 100 mg/L, 40 mL of Rh-B solution was added to seven beakers, then 40 mg of adsorbent was added to each beaker. The adsorption times were set in the seven beakers as 5, 10, 20, 30, 60, 90, and 120 min, respectively.

2.4.3. Effect of pH

At the normal temperature with an initial concentration of 100 mg/L, 40 mL of Rh-B solution was added to six beakers; then 40 mg of adsorbent was added to each beaker; however, the pH of Rh-B solution in the six beakers was adjusted by hydrochloric acid and sodium hydroxide solution to be 4, 6, 7, 8, 10, and 12, respectively, and the adsorption time was set for 60 min.

2.4.4. Effect of the Absorbent Dosage

At the normal temperature with the initial concentration of 100 mg/L, 40 mL of Rh-B solution was added to six beakers, then the dosage of adsorbent was introduced in the six beakers as 10, 20, 30, 40, 50, and 60 mg, respectively, and the adsorption time was set for 60 min.

3. Results and Discussion

3.1. Characterization of Adsorbents

3.1.1. XRD Analyses

It can be seen from Figure 3a that using CTAB modified MAG could effectively expanded its layer spacing, from original 1.52 nm to 3.166 nm, because CTAB can be inserted into the inter-layer of the MAG; meanwhile, the reflection at 5.809° was still visible, indicating that a small portion of MAG was still not intercalated by CTAB. However, the diffraction peak at 2.788° was higher than the diffraction peak at 5.809°, indicating that the intercalation rate was high, which met the needs of this experiment. The enlargement of the layer spacing means that there will be more space between the layers, which can absorb more pollutants.

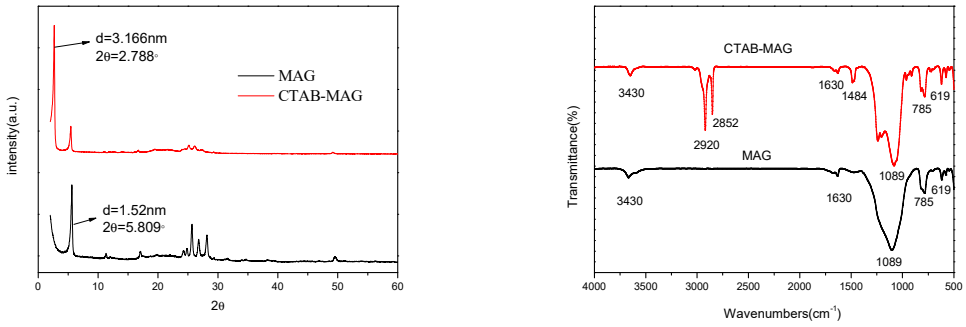

(**a**) (**b**)

Figure 3. Patterns of MAG and cetyltrimethylammonium-bromide (CTAB)-MAG (**a**) XRD and (**b**) FTIR.

3.1.2. FTIR Analyses

Figure 3b shows that the absorption reflection bands at 3430 cm^{-1} and 1630 cm^{-1} belong to the stretching and bending vibration of the O–H bond; the absorption reflection band at 1089 cm^{-1} belongs to the symmetric stretching vibration of the [SiO_4] tetrahedron; the absorption reflection bands at 785 cm^{-1} and 619 cm^{-1} belong to the double rings vibrations. However, CTAB-MAG has three more absorption peaks (at bands 2920 cm^{-1}, 2852 cm^{-1}, and 1484 cm^{-1}) than the MAG spectrum; the symmetric vibration of C–H functional groups belong to the absorption reflection band at 2920 cm^{-1}; the asymmetric vibration of C–H functional groups belong to the absorption reflection band at 2852

cm-1; however, the bending vibration of C–H functional groups belong to the absorption reflection band at 1484 cm^{-1}, thus those results can be proof that MAG and CTAB were presented in the CTAB-MAG sample. Therefore, the addition of CTAB does not destroy the structure of MAG. Combined with XRD analysis, we can prove that CTAB was inserted into the MAG interlayer, thereby increasing the layer spacing of CTAB-MAG.

3.1.3. SEM Analysis

Figure 4 shows the SEM images of MAG and CTAB-MAG. The particles of MAG were rose petal-like and the particle size was nanometer grade in the z direction; however, the particle size was micrometer grade in two other directions (shown in Figure 4a) while part of the laminate of CTAB-MAG was stripped because of the change of layer spacing (shown in Figure 4b).

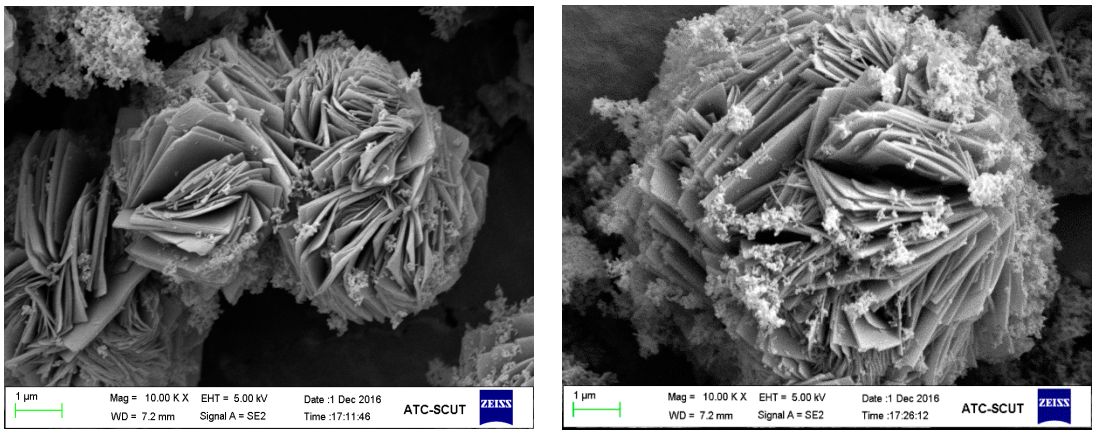

(**a**) (**b**)

Figure 4. SEM image of (**a**) MAG and (**b**) CTAB-MAG.

3.2. Adsorption Performance

3.2.1. Influencing Factors of the Adsorption Capacity

As can be seen from Figure 5a, the adsorption capacity of MAG and CTAB-MAG increased from 21.79 mg/g to 57.87 mg/g, and 27.16 mg/g to 77.68 mg/g with the increasing of the initial concentration of Rh-B from 30 mg/L to 150 mg/L. This was because with the increasing of the initial concentration of Rh-B, the mass transfer power to the adsorbent increases, resulting in an adsorption capacity increase. As can be seen from Figure 5b, the adsorption capacity of MAG and CTAB-MAG increased quickly from 31.85 mg/g to 46.56 mg/g, and from 45.36 mg/g to 65.34 mg/g with the increase of the adsorption time from 5 min to 40 min; however, the adsorption capacity of MAG and CTAB-MAG increased slowly from 46.56 mg/g to 49.07 mg/g, and 65.34 mg/g to 68.82 mg/g with the increase of adsorption time from 40 min to 120 min, respectively. The reason is that the adsorption capacity was increased rapidly first and then increased slowly. The active site of adsorbent was decreased gradually with the adsorption process; on the other hand, the concentration of Rh-B in the solution was gradually decreased; therefore, the rate of particle diffusion was promoted by the concentration difference decreases, resulting in the decrease of the adsorption rate. Figure 5c shows that the adsorption capacity of MAG and CTAB-MAG decreased quickly from 52.39 mg/g to 34.90 mg/g, and from 84.12 mg/g to 40.52 mg/g with the increasing of the pH from 4 to 12, respectively. This decrease could be attributed to competition between the Rh-B dye molecules and the hydroxyl ions present at these pH values [32]. Figure 5d shows that the adsorption capacity of MAG and CTAB-MAG decreased quickly from 128.52 mg/g to 35.54 mg/g, and 149.24 mg/g to 52.43 mg/g with the increasing of the dosage of MAG and CTAB-MAG from 0.25 g/L to 1.5 g/L, respectively.

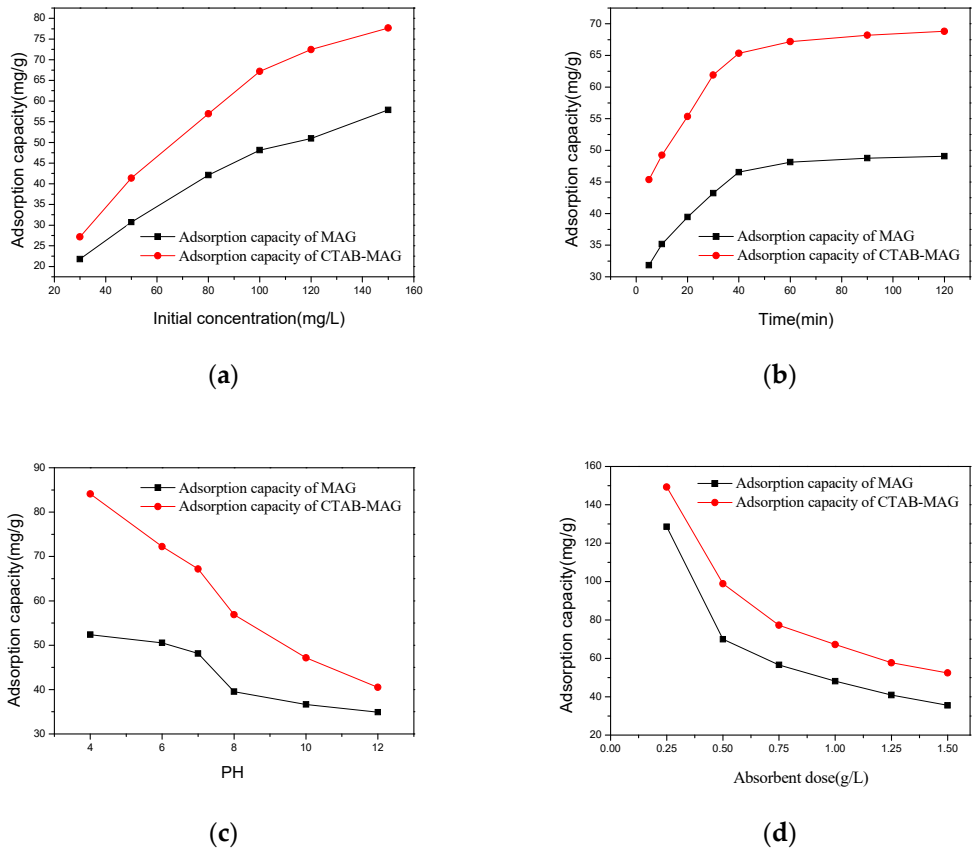

Figure 5. Factors affecting adsorption capacity: (**a**) Initial concentration, (**b**) adsorption time, (**c**) pH, and (**d**) absorbent dosage.

3.2.2. Isothermal Adsorption Experiment

The adsorption capacity was fitting by the Langmuir model equation and the Freundlich model equation [33,34], as shown in Equations (3) and (4).

$$q_e = \frac{K_L q_{\max} C_e}{1 + K_L C_e} \tag{3}$$

where C_e is the concentration at equilibrium (mg·L^{-1}), q_e is the adsorption capacity when the adsorption balance (mg·g^{-1}), and K_L is Langmuir equilibrium constant (L·mg^{-1}).

$$q_e = K_F C_e^n \tag{4}$$

where K_F and n are the Freundlich equilibrium constant and the characteristic constant, respectively. Figure 6 shows that the adsorption capacity was fitted by Langmuir model equation and Freundlich model equation; meanwhile, Table 1 shows that the related parameters had been well presented. By using the Langmuir model, the correlation coefficients (R^2) for MAG and CTAB-MAG were found—0.99 and 0.993, respectively; however, by using the Freundlich model, the correlation coefficients (R^2) for MAG and CTAB-MAG were found to be 0.984 and 0.987, respectively, thus indicting that the Langmuir model and Freundlich model can simulate the adsorption process together. However, the Freundlich model constants (1/n) for MAG and CTAB-MAG were found to be 0.40486 and 0.32086, respectively. They were less than 1, indicating an adsorption process consist with monolayer adsorption; meanwhile, this conclusion is also consisted with the assumptions of the Langmuir model.

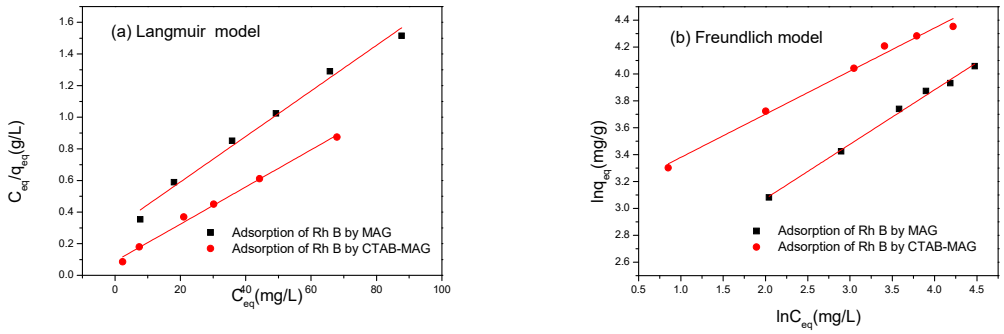

(**a**) (**b**)

Figure 6. Adsorption isotherm models. (**a**) Langmuir model, and (**b**) Freundlich model.

Table 1. Isotherm adsorption equation fitted parameters.

	Langumir Model			**Freundlich Model**		
	$\mathbf{K_L}$	$\mathbf{q_m}$	$\mathbf{R^2}$	$\mathbf{K_F}$	**1/n**	$\mathbf{R^2}$
MAG	0.0476	69.44	0.99718	9.611	0.40486	0.98432
CTAB-MAG	0.1321	85.11	0.99327	21.304	0.32086	0.98763

3.2.3. Adsorption Kinetics Model

The adsorption capacity was fitted by the pseudo first order dynamic equation and the pseudo second order dynamic equation [35–37], as shown in Equations (5) and (6). Equation (5) was the pseudo first order dynamic equation expression.

$$q_t = q_{\mathrm{eq}}\left(1 - e^{-k_1 t}\right) \tag{5}$$

where K_1 was pseudo first order rate constants(min^{-1}), q_{eq} was the adsorption capacity when the adsorption balance($\mathrm{mg{\cdot}g^{-1}}$), and q_t was the adsorption capacity when the time was t ($\mathrm{mg{\cdot}g^{-1}}$). Equation (6) was the pseudo second order dynamic equation expression.

$$q_t = \frac{k_2 q_{\mathrm{eq}}^2 t}{1 + k_2 q_{eq} t} \tag{6}$$

where K_2 is the pseudo second order rate constants ($\mathrm{g{\cdot}mg^{-1}{\cdot}min^{-1}}$), q_{eq} is the adsorption capacity when the adsorption reached at equilibrium ($\mathrm{mg{\cdot}g^{-1}}$), and q_t is the adsorption capacity at time t ($\mathrm{mg{\cdot}g^{-1}}$). Figure 7 shows that the adsorption capacity was fitted by of the pseudo first order kinetic model and the pseudo second order kinetic model; meanwhile, Table 2 shows that the related parameters had been well presented. By using of the pseudo second order kinetic model, the correlation coefficients (R^2) for MAG and CTAB-MAG were found to be 0.999 and 0.999, respectively; however, by using the pseudo first order kinetic model, the correlation coefficients (R^2) for MAG and CTAB-MAG were 0.988 and 0.979, respectively, thus the correlation coefficients (R^2) of the pseudo second order kinetic model were larger than the correlation coefficients (R^2) of the pseudo first order kinetic model for MAG and CTAB-MAG. Therefore, it indicates that the pseudo second order kinetic model was more appropriate for describing the adsorption process.

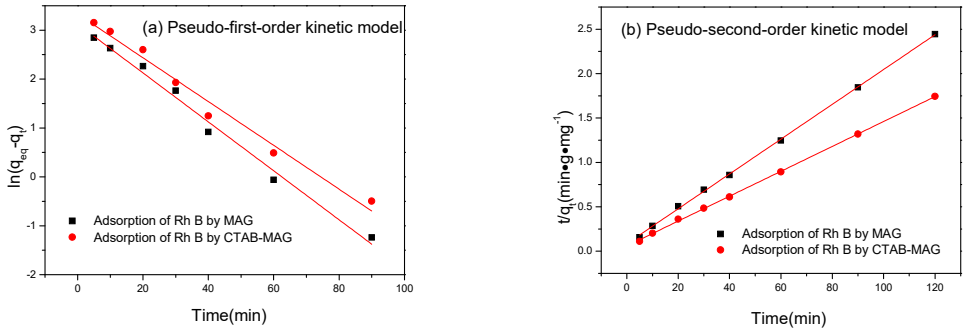

(**a**) (**b**)

Figure 7. Kinetic curves. (**a**) Pseudo-first-order kinetic model, and (**b**) pseudo-second-order kinetic model.

Table 2. Adsorption kinetic constants of Rh-B.

	Pseudo-First-Order Kinetic Model			**Pseudo-Second-Order Kinetic Model**			**Experiment**
	K_1	q_{eqc}	R^2	K_2	q_{eqc}	R^2	q_{eqe}
MAG	0.0501	22.81	0.98817	0.00449	50.994	0.99937	49.07
CTAB-MAG	0.0448	27.99	0.97913	0.00336	71.327	0.99949	68.82

The Table 2 shows that the experimental results (q_{eqe}) of MAG and CTAB-MAG were 49.07 and 68.82, respectively. The calculated results (q_{eqc}) for the pseudo-second-order dynamic equation of MAG and CTAB-MAG were 50.994 and 71.327, respectively; however, the calculated results (q_{eqc}) for the pseudo first order dynamical equation of MAG and CTAB-MAG were 22.81 and 27.99, respectively. Thus, the calculated results (q_{eqc}) of the pseudo-second-order dynamic equation approached the investigational results (q_{eqe}) indicting that the pseudo-second-order kinetic model was more appropriate for relating the adsorption process.

3.2.4. Adsorption Ratio Model

In order to investigate the adsorption rate, we research the dynamic boundary models, such as the film diffusion model, particle diffusion model, and chemical reaction model. We defined q_t/q_{eq} as F, where q_t was the adsorption capacity at time t ($mg \cdot g^{-1}$), and q_{eq} was the adsorption capacity when the adsorption reached equilibrium ($mg \cdot g^{-1}$), in the three equations that follow [38,39].

Film diffusion model:

$$-\ln(1-F) = kt \tag{7}$$

Particle diffusion model:

$$1 - 3(1-F)^{\frac{2}{3}} + 2(1-\mathrm{F}) = kt \tag{8}$$

Chemical reaction model:

$$1 - (1-F)^{\frac{1}{3}} = kt \tag{9}$$

Figure 8 shows the three moving boundary models. Figure 8a is the film diffusion; 8b is the particle diffusion; 8c is the chemical reaction. The results of the moving boundary models have been presented in Table 3. As shown in Table 3, the correlation coefficients R^2 of the film diffusion model for MAG (0.988) and CTAB-MAG (0.979) were larger than in the particle diffusion model for MAG (0.909) and CTAB-MAG (0.887), as well as chemical reaction model for MAG (0.934) and CTAB-MAG (0.911), indicating that the film diffusion was more suitable for describing the adsorption.

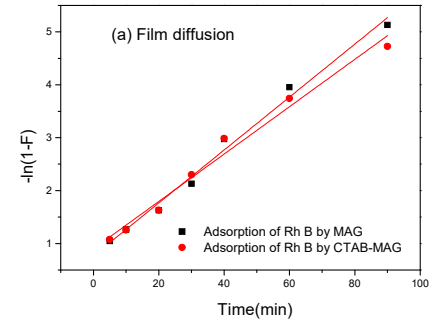

(**a**)

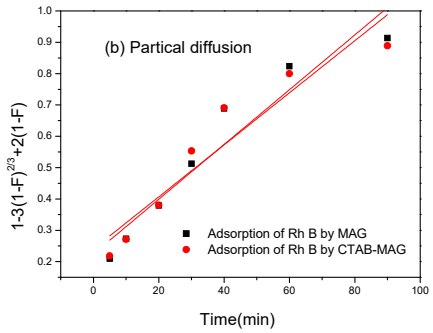

(**b**)

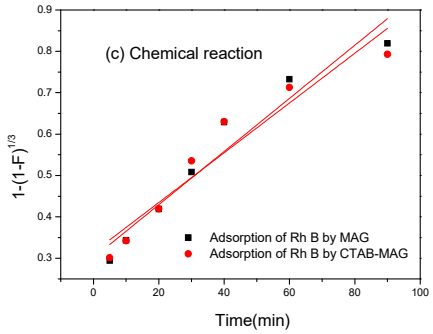

(**c**)

Figure 8. Moving boundary models. (**a**) Film diffusion, (**b**) particle diffusion, and (**c**) chemical reaction.

Table 3. Equation constants of moving boundary models.

	Film Diffusion		**Particle Diffusion**		**Chemical Reaction**	
	k	**R^2**	**k**	**R^2**	**k**	**R^2**
MAG	0.051	0.988	0.009	0.909	0.006	0.934
CTAB-MAG	0.045	0.979	0.008	0.887	0.006	0.911

3.2.5. The Greater Adsorption Performance of CTAB-MAG

The adsorption capacities of MAG and CTAB-MAG were 48.13 mg/g, 67.19 mg/g, respectively. When pH was 7, adsorption time was 60 min, the initial concentration of Rh-B was 100 mg/L, and the adsorbent dosage was 1 g/L. The Table 4 shows that the adsorption capacity of MAG (48.13 mg/g) and CTAB-MAG (67.19 mg/g) were both higher than kaolinite (46.08 mg/g) [40], sodium montmorillonite

(42.19 mg/g) [41], and duolite C-20 resin (28.57 mg/g) [42]. Those results indicate in this process that CTAB-MAG can be used as an efficient low-cost adsorbent for removing Rh-B from an aqueous solution.

Table 4. Comparison of Rh-B adsorption capacity with other reported systems.

Adsorbents	Conditions	Isotherms	Kinetics	Adsorption Capacity	References
CTAB-MAG	Ph = 7; dosage 1 g/L; Rh-B concentration 100 mg/L	Langmuir and Freundlich	pseudo-second-order	67.19 mg/g	This work
MAG	Ph = 7; dosage 1 g/L; Rh-B concentration 100 mg/L	Langmuirand Freundlich	pseudo-second-order	48.13 mg/g	This work
Kaolinite	Ph = 7; dosage 3 g/L; Rh-B concentration 90 mg/L	Langmuir	pseudo-second-order	46.08 mg/g	[40]
Sodium montmorillonite	Ph = 7; dosage 0.3 g/L; Rh-B concentration 200 mg/L	Langmuir	pseudo-second-order	42.19 mg/g	[41]
Duolite C-20 resin	Ph = 7; dosage 0.4 g/L; Rh-B concentration 8.129 mg/L	Langmuir and Freundlich	pseudo-first-order	28.57 mg/g	[42]

4. Conclusions

In this work, we prepared CTAB-MAG by using CTAB to modify MAG, based on ion exchange. Compared with MAG, CTAB-MAG can effectively increase the layer spacing of MAG from 1.52 nm to 3.166 nm, thereby enhancing its adsorption capacity. Meanwhile, the adsorption results shown the pronounced affinity of the CTAB-MAG to the Rh-B dye molecules. The adsorption capacities of MAG and CTAB-MAG were 48.13 mg/g and 67.19 mg/g. The adsorption capacity of CTAB-MAG was increased by 40% over MAG, indicating that CTAB-MAG can be used as an efficient, low-cost adsorbent. The pseudo-second-order kinetic equation was more suitable for describing the adsorption; the adsorption process was dominated by a film diffusion process. The adsorption process belongs to monomolecular layer adsorption processes.

Author Contributions: Conceptualization, M.G., C.Z., and G.L.; data curation, Y.Y., L.J., and J.A.S.M.; formal analysis, Z.X.; funding acquisition M.G., G.L., and Y.Y.; investigation, M.G., Z.X., C.Z., and G.L.; methodology, Z.X., C.Z., and G.L.; project administration, M.G.; resources, Y.Y. and G.H.; software, J.A.S.M. and L.J.; supervision, M.G.; validation, C.Z. and J.A.S.M.; visualization, Z.X. and J.A.S.M.; writing—original draft, Z.X.; writing—reviewing and editing, G.H., L.J., and J.A.S.M.

Funding: The authors gratefully acknowledge the financial support of this research work by the Natural Science Foundation of Guangdong Province Project (project number 2016A030313520), Key Laboratory of Polymeric Composite and Functional Materials of Ministry of Education Project (project number PCFM-2017-02), Guangdong Water Conservancy Science and Technology Innovation Project (project number 2017-24), and the Guangdong Provincial Department of Education Featured Innovation Project (project number 2017KTSCX007).

Acknowledgments: The authors are grateful to the reviewers for their valuable review comments to enrich the publication.

Conflicts of Interest: The authors declare no conflict of interest. The funders had no role in the design of the study; in the collection, analyses, or interpretation of data; in the writing of the manuscript, and in the decision to publish the results.

References

1. Baddouh, A.; Garcia Bessegato, G.; Rguiti, M.M.; EI Ibrahimi, B.; Bazzi, L.; Hilali, M.; Boldrin Zanoni, M.V. Electrochemical decolorization of Rhodamine B dye: Influence of anode material, chloride concentration and current density. *J. Environ. Chem. Eng.* **2018**, *6*, 2041–2047. [CrossRef]
2. Zeng, H.X.; Zhang, W.Q.; Deng, L.; Luo, J.M.; Zhou, S.Q.; Liu, X.; Pei, Y.; Shi, Z.; Crittenden, J. Degradation of dyes by peroxymonosulfate activated by ternary CoFeNi-layered double hydroxide: Catalytic performance, mechanism and kinetic modeling. *J. Colloid Interface Sci.* **2018**, *515*, 92–100. [CrossRef] [PubMed]
3. Isari, A.A.; Payan, A.; Fattahi, M.; Jorfi, S.; Kakavandi, B. Photocatalytic degradation of rhodamine B and real textile wastewater using Fe-doped TiO_2 anchored on reduced graphene oxide (Fe-TiO_2/rGO): Characterization and feasibility, mechanism and pathway studies. *Appl. Surf. Sci.* **2018**, *462*, 549–564. [CrossRef]

4. Qiu, L.Y.; Wang, Q.Y.; Liu, Z.Y.; Zhao, Q.Q.; Tian, X.Y.; Li, H.L.; Gao, S.M. Preparation of 3D TiO_2 nanotube arrays photoelectrode on Ti mesh for photoelectric conversion and photoelectrocatalytic removal of pollutant. *Sep. Purif. Technol.* **2018**, *207*, 206–212. [CrossRef]
5. Liang, C.; Liu, Y.H.; Li, K.; Wen, J.; Xing, S.T.; Ma, Z.C.; Wu, Y.S. Heterogeneous photo-Fenton degradation of organic pollutants with amorphous Fe-Zn-oxide/hydrochar under visible light irradiation. *Sep. Purif. Technol.* **2017**, *188*, 105–111. [CrossRef]
6. Li, L.; Iqbal, J.; Zhu, Y.; Zhang, P.; Chen, W.C.; Bhatnagar, A.; Du, Y.P. Chitosan/Ag-hydroxyapatite nanocomposite beads as a potential adsorbent for the efficient removal of toxic aquatic pollutants. *Int. J. Biol. Macromol.* **2018**, *120*, 1752–1759. [CrossRef]
7. Eugster, H.P. Hydrous sodium silicates from Lake Magadi, Kenya: Precursors of bedded chert. *Science* **1967**, *157*, 1177–1180. [CrossRef]
8. Homhuan, N.; Bureekaew, S.; Ogawa, M. Efficient Concentration of Indium (III) from Aqueous Solution Using Layered Silicates. *Langmuir* **2017**, *33*, 9558–9564. [CrossRef]
9. Kooli, F.; Liu, Y.; Abboudi, M.; Rakass, S.; Hassani, H.O.; Ibrahim, S.M.; Al-Faze, R. Application of Organo-Magadiites for the Removal of Eosin Dye from Aqueous Solutions: Thermal Treatment Regeneration. *Molecules.* **2018**, *23*, 2280. [CrossRef]
10. Zhang, Y.F.; Wang, Q.S.; Gao, S.N.; Jiang, H.M.; Meng, C.G. Intercalation and in situ formation of coordination compounds with ligand 8-hydroxyquinoline-5-sulfonic acid in the interlayer space of layered silicate magadiite by solid-solid reactions. *Microporous Mesoporous Mater.* **2018**, *266*, 14–23. [CrossRef]
11. Mao, Y.T.; Li, S.G.; Fang, R.L.; Ploehn, H.J. Magadiite/styrene-butadiene rubber composites for tire tread applications: Effects of varying layer spacing and alternate inorganic fillers. *J. Appl. Polym. Sci.* **2017**, *134*, 44764. [CrossRef]
12. Li, S.G.; Mao, Y.T.; Ploehn, H.J. Interlayer functionalization of magadiite with sulfur-containing organosilanes. *Colloids Surf. A Physicochem. Eng. Asp.* **2016**, *506*, 320–330. [CrossRef]
13. Wang, Q.S.; Zhang, Y.F.; Zheng, J.Q.; Hu, T.; Meng, C.G. Synthesis, structure, optical and magnetic properties of interlamellar decoration of magadiite using vanadium oxide species. *Microporous Mesoporous Mater.* **2017**, *244*, 264–277. [CrossRef]
14. Ge, M.L.; Cao, L.X.; Du, M.Y.; Hu, G.Q.; Jahangir Alam, S.M. Competitive adsorption analyses of a pure magadiite and a new silylated magadiite on methylene blue and phenol from related aqueous solution. *Mater. Chem. Phys.* **2018**, *217*, 393–402. [CrossRef]
15. Lim, W.T.; Jang, J.H.; Park, N.Y.; Paek, S.M.; Kim, W.C.; Park, M. Spontaneous nanoparticle formation coupled with selective adsorption in magadiite. *J. Mater. Chem. A* **2017**, *5*, 4144–4149. [CrossRef]
16. Kosuge, K.; Yamazaki, A.; Tsunashima, A.; Otsuka, R. Hydrothermal synthesis of magaditte and kenyaite. *J. Ceram. Soc. Jpn.* **1992**, *100*, 326–331. [CrossRef]
17. Wang, Y.R.; Wang, S.F.; Chang, L.C. Hydrothermal synthesis of magadiite. *Appl. Clay Sci.* **2006**, *33*, 73–77. [CrossRef]
18. Kwon, O.Y.; Park, K.W. Synthesis of layered silicates from sodium silicate solution. *Bull. Korean Chem. Soc.* **2004**, *25*, 25–26.
19. Jeong, S.Y.; Kwon, O.Y.; Suh, J.K.; Jin, H.; Lee, J.M. Preparation of silica-pillared molecular sieves from layered silicates. *Stud. Surf. Sci. Catal.* **1997**, *105*, 53–60.
20. Zhao, J.; Zhang, Y.F.; Zhang, S.Q.; Wang, Q.S.; Chen, M.; Hu, T.; Meng, C.G. Synthesis and characterization of Mn-Silicalite-1 by the hydrothermal conversion of Mn-magadiite under the neutral condition and its catalytic performance on selective oxidation of styrene. *Microporous Mesoporous Mater.* **2018**, *268*, 16–24. [CrossRef]
21. Ge, M.L.; Chen, M. Preparation and Characterization of Magadiite. *J. Chin. Ceram. Soc.* **2013**, *42*, 1704–1708.
22. Ge, M.L.; Wang, Y.W.; Chen, M. Adsorption Characteristics of Zn^{2+} onto Magadiite. *China Environ. Sci.* **2015**, *35*, 2065–2071.
23. Ge, M.L.; Wang, X.B.; Du, M.Y.; Liang, G.D.; Hu, G.Q.; Jahangir Alam, S.M. Effect on the mechanical properties of nacre-like bio-hybrid membranes with inter-penetrating petal structure based on magadiite. *Materials* **2019**, *12*, 173. [CrossRef] [PubMed]
24. Ge, M.L.; Tang, W.; Du, M.Y.; Liang, G.D.; Hu, G.Q.; Jahangir Alam, S.M. Research on 5-fluorouracil as drug carrier materials with its in vitro release properties on organic modified magadiite. *Eur. J. Pharm. Sci.* **2019**, *130*, 44–53. [CrossRef] [PubMed]

25. Peng, S.; Gao, Q.; Wang, Q.G.; Shi, J.L. Layered Structural Heme Protein Magadiite Nanocomposites with High Enzyme-like Peroxidase Activity. *Chem. Mater.* **2004**, *16*, 2675–2684. [CrossRef]
26. Kooli, F.; Yan, L. Thermal Stable Cetyltrimethylammonium-Magadiites: Influence of the Surfactant Solution Type. *J. Phys. Chem. C* **2009**, *113*, 1947–1952. [CrossRef]
27. Kooli, F.; li, M.; Alshahateet, S.F.; Chen, F.X.; Zhu, Y.H. Characterization and thermal stability properties of intercalated Na-magadiite with cetyltrimethylammonium (C_{16}TMA) surfactants. *J. Phys. Chem. Solids* **2006**, *67*, 926–931. [CrossRef]
28. Macedo, T.R.; Airoldi, C. Host lamellar silicic acid magadiite for some heterocyclic amine inclusions and quantitative calorimetric data. *Microporous Mesoporous Mater.* **2006**, *94*, 81–88. [CrossRef]
29. Park, K.W.; Jung, J.H.; Kim, S.K.; Kwon, O.Y. Interlamellar silylation of magadiite by octyl triethoxysilane in the presence of dodecylamine. *Appl. Clay Sci.* **2009**, *46*, 251–254. [CrossRef]
30. Ge, M.L.; Du, M.Y.; Zheng, L.Y.; Wang, B.Y.; Zhou, X.Y.; Jia, Z.X.; Hu, G.Q.; Jahangir Alam, S.M. A maleic anhydride grafted sugarcane bagasse adsorbent and its performance on the removal of methylene blue from related wastewater. *Mater. Chem. Phys.* **2017**, *192*, 147–155. [CrossRef]
31. Ge, M.L.; Cao, L.X.; Du, M.Y.; Hu, G.Q.; Jahangir Alam, S.M. Adsorption characterization of a pure magadiite and an organic modified magadiite on removal of methylene blue from related aqueous solution. *Mater. Chem. Phys.* **2018**, *217*, 533–540. [CrossRef]
32. Mokhtar, M. Application of Synthetic Layered Sodium Silicate Magadiite Nanosheets for Environmental Remediation of Methylene Blue Dye in Water. *Materials* **2017**, *10*, 760. [CrossRef] [PubMed]
33. Detrich, A.; Deak, A.; Hild, E.; Kovacs, A.L.; Horvolgyi, Z. Langmuir and Langmuir-Blodgett Films of Bidisperse Silica Nanoparticles. *Langmuir* **2010**, *26*, 2694–2699. [CrossRef] [PubMed]
34. Factorovich, M.H.; Solveyra, E.G.; Molinero, V. Sorption isotherms of Water in Nanopores: Relationship Between Hydropohobicity, Adsorption Pressure, and Hysteresis. *J. Phys. Chem. C* **2014**, *118*, 16290–16300. [CrossRef]
35. Chen, F.F.; Liu, Q.J.; Xu, Z.M.; Sun, X.W.; Shi, Q.; Zhao, S.Q. Adsorption Kinetics and Thermodynamics of Vanadyl Etioporphyrin on Asphaltene in Pentane. *Energy Fuels* **2013**, *27*, 6408–6418. [CrossRef]
36. Kumar, K.V.; Khaddour, I.A.; Gupta, V.K. A Pseudo Second-Order Kinetic Expression for Dissolution Kinetic Profiles of Solids in Solutions. *Ind. Eng. Chem. Res.* **2010**, *49*, 7257–7262. [CrossRef]
37. Ge, M.L.; Wang, X.B.; Du, M.Y.; Liang, G.D.; Hu, G.Q.; Jahangir Alam, S.M. Adsorption analyses of phenol from aqueous solution using magadiite modified with organo-functional groups: Kinetic and equilibrium studies. *Materials* **2019**, *12*, 96. [CrossRef] [PubMed]
38. Guerra, D.J.L.; Mello, I.; Resende, R.; Silva, R. Application as absorbents of natural and functionalized Brazilian bentonite in Pb^{2+} adsorption: Equilibrium, kinetic, pH, and thermodynamic effects. *Water Resour. Ind.* **2013**, *4*, 32–50. [CrossRef]
39. Ge, M.L.; Xi, Z.Z.; Zhu, C.P.; Liang, G.D.; Hu, G.Q.; Jamal, L.; Jahangir Alam, S.M. Preparation and characterization of magadiite-magnetite nanocomposite with its sorption performance analyses on removal of methylene blue from aqueous solution. *Polymers* **2019**, *11*, 607. [CrossRef]
40. Khan, T.A.; Dahiya, S.; Ali, I. Use of kaolinite as adsorbent: Equilibrium, dynamics and thermodynamic studies on the adsorption of rhodamine B from aqueous solution. *Appl. Clay Sci.* **2012**, *69*, 58–66. [CrossRef]
41. Selvam, P.P.; Preethi, S.; Basakaralingam, P.; Thinakaran, N.; Sivasamy, A.; Sivanesan, S. Removal of rhodamine B from aqueous solution by adsorption onto sodium montmorillonite. *J. Hazard. Mater.* **2008**, *155*, 39–44. [CrossRef] [PubMed]
42. Al-Rashed, S.M.; Al-Gaid, A.A. Kinetic and thermodynamic studies on the adsorption behavior of rhodamine B dye on duolite C-20 resin. *J. Saudi Chem. Soc.* **2012**, *16*, 209–215. [CrossRef]